

## Toroidal Alfvén Eigenmode Avalanches in NSTX

E. D. Fredrickson 1), N. A. Crocker 2), D. Darrow 1), N. N. Gorelenkov 1),  
 W. W. Heidbrink 3), G. J. Kramer 1), S. Kubota 2), B. LeBlanc 1), F. M. Levinton 4),  
 D. Liu 3), S. S. Medley 1), J. Menard 1), W. A. Peebles 2), M. Podesta 3), R. B. White  
 1), H. Yuh 4), R. E. Bell 1)

1) Princeton Plasma Physics Laboratory, Princeton New Jersey 08543

2) Univ. of California, Los Angeles, CA 90095

3) Univ. of California., Irvine, CA 92697

4) Nova Photonics, Princeton, NJ 08543

email contact of main author: [efredrickson@pppl.gov](mailto:efredrickson@pppl.gov)

**Abstract.** The transport of fast-ions resulting from strongly non-linear Toroidal Alfvén Eigenmode avalanches has been studied experimentally and simulated with the NOVA ideal MHD code and the ORBIT code to model fast ion transport. Detailed measurements of the multi-mode structure and amplitudes have been made to benchmark NOVA calculations of eigenmodes. The ORBIT code has been used to model the fast-ion transport, and good agreement has been found with experimental measurements with the NPA and fast neutron rate diagnostics.

### 1. Introduction

The National Spherical Torus Experiment (NSTX) is a beam heated, low aspect ratio ( $R/a \approx 1.3$ ) tokamak [1]. NSTX is typically operated with  $\approx 1$  MA of plasma current, a minor cross-sectional area of  $\approx 2.4$  m<sup>2</sup>, and a toroidal field of  $\approx 4.5$  kG. These parameters provide good confinement of deuterium beam ions with energies up to 90 kV. For the typical range of NSTX plasma densities, the ratio of the full energy beam-ion velocity to the Alfvén speed is  $V_{\text{beam}}/V_{\text{Alfvén}} \approx 1-5$ , providing strong drive for Alfvénic instabilities.

Since the discovery of Toroidal Alfvén Eigenmodes (TAE) over 15 years ago, considerable progress has been made towards developing a predictive capability for the linear stability and structure of these instabilities [2]. Advances in computing technology and theoretical understanding have now opened the possibility of extending this knowledge to include a predictive capability for the nonlinear behavior of these modes. The nonlinear numerical codes, such as M3D-k, and theoretical models will need to be benchmarked against detailed experimental data on mode structure, amplitudes and fast ion transport from studies of TAE and other beam driven instabilities. In this paper we will describe detailed experimental measurements of equilibrium quantities, internal mode structure and fast ion transport during TAE avalanches [3,4]. We will also present some of the data and analysis demonstrating a second example of non-linear behavior, the three-wave coupling of TAE to an energetic particle mode (EPM) [4].

TAE avalanches as seen in Fig. 1 are an example of the nonlinear interaction of multiple modes. When multiple modes, with resonances closely spaced in phase space, reach a sufficient amplitude that the fast ion trajectories overlap, very rapid non-linear growth can occur. The modification of the fast ion distribution by this loss may in turn excite additional, otherwise stable, modes, leading to an “avalanche” effect and greatly enhancing the transport of fast ions [3]. This type of nonlinear multimode interaction is a topic of concern for ITER where, due to small  $\rho^*$  (ratio of ion Larmor radius to plasma

radius), any significant fast ion transport from TAE is expected to be through multimode processes.

## 2. Experimental conditions for study of TAE avalanches

TAE avalanches are seen in both L-mode and H-mode beam heated plasmas on NSTX. The target plasmas for these experiments were nominally He plasmas (which raises the threshold power needed to trigger H-modes) heated with deuterium neutral beams. The L-mode density profiles were necessary for the reflectometer measurements of the internal mode structure. The thresholds for excitation of TAE and TAE avalanches were experimentally identified by starting from quiescent plasmas at low  $\beta_{fast}$  and increasing the beam power until first TAE and then TAE avalanches were found.

Plasma parameters were measured with an array of diagnostics, notably charge-exchange recombination spectroscopy (CHERS) for ion temperature, toroidal rotation and carbon density profiles (the dominant impurity for  $Z_{eff}$ ), Thomson scattering (TS) for electron density and temperature profiles and motional Stark

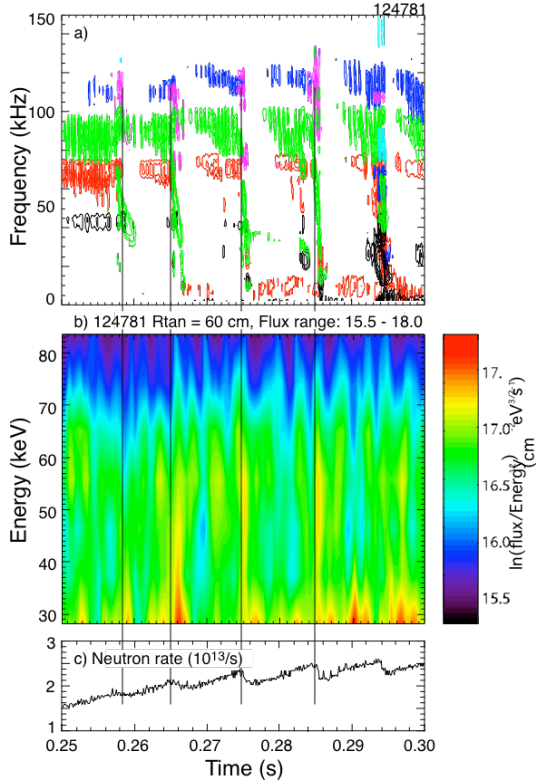


Fig. 1 a) Spectrogram of Mirnov coil showing TAE modes: color indicates toroidal mode number (black – 1, red – 2, green – 3, blue – 4, magenta – 6), b) particle flux vs. time and energy from ssNPA chord lookiwith tangency radius of 60 cm, c) neutron rate.

effect (MSE) for magnetic field pitch angle profiles to constrain equilibrium reconstructions. The MSE diagnostic requires neutral beam source A (tangency radius 69.2 cm) at 90 kV, so experiments were designed to take MSE measurements before and after the time of interest, and similar shots were taken with MSE measurements at the time of interest.

## 3. External and internal measurements of mode structure and amplitude

Mirnov coils mounted on the vacuum vessel wall are used to measure the frequency spectrum and toroidal wavelengths for the individual TAE instabilities. A spectrogram of magnetic fluctuations is shown in Fig. 1a. The spectrogram covers the time range from roughly the onset of TAE activity until the onset of fishbone modes (when  $q(0)$  drops to one). Five strong TAE bursting events are seen; these bursts are identified as TAE avalanches and are correlated with drops of order 10% in the neutron rate. Following each burst, the TAE are quiescent for a short period, then increase in amplitude until the next strong burst. The final avalanche is accompanied by a strong  $n=1$  fishbone mode, indicating a coupling of TAE and fishbone energetic particle modes.

The five fixed-frequency heterodyne and quadrature reflectometers are the primary diagnostic used for internal measurements of the TAE structure. The frequencies for the reflectometers are 30, 35, 42, 44.5 and 50 GHz, corresponding to electron densities at the

cut-off layers of 1.12, 1.52, 2.19, 2.46 and 3.1  $\times 10^{19}/\text{m}^3$ , respectively. The density profile, and corresponding locations of the cut-off layers (black dots) are shown in Fig. 2, together with the q-profile showing weak reversed shear.

In Fig. 3a and 3d are shown spectrograms of the density and magnetic fluctuations as measured with the 50 GHz reflectometer channel and the Mirnov coil array, respectively, covering a single avalanche cycle. The dominant mode is the  $n=3$  (green), with weaker  $n=2$  and 4 modes. In the final burst an  $n=6$  and  $n=9$  mode also appear.

The normalized total rms fluctuation amplitude over the frequency range from

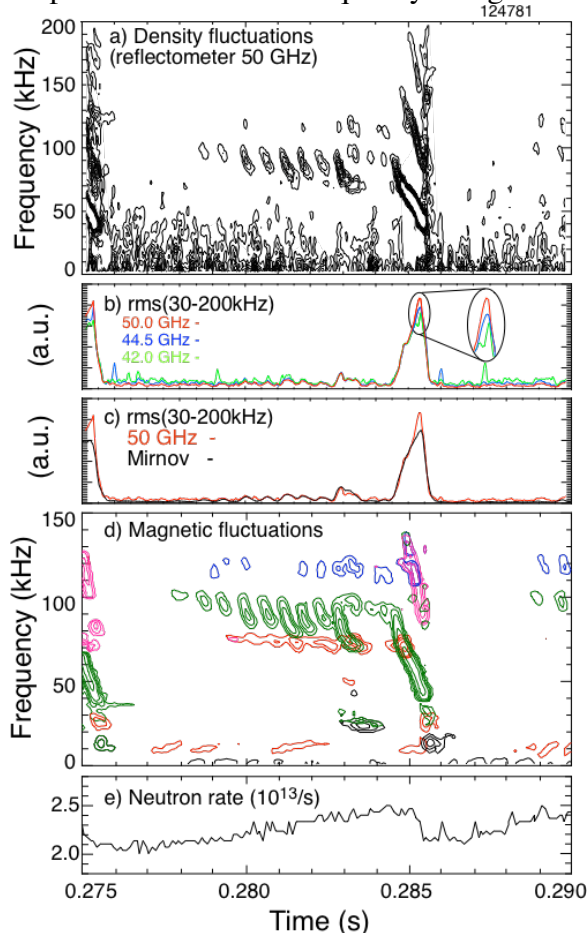


Fig. 3 a) Detail spectrogram of single avalanche cycle 50GHz reflectometer. b) overlaid RMS amplitude of three core reflectometer channels, c) rms amplitude of core reflectometer and a Minrov coil, d) spectrogram of magnetic fluctuations showing TAE, colors as in Fig. 1, e) neutron rate showing drop at avalanche.

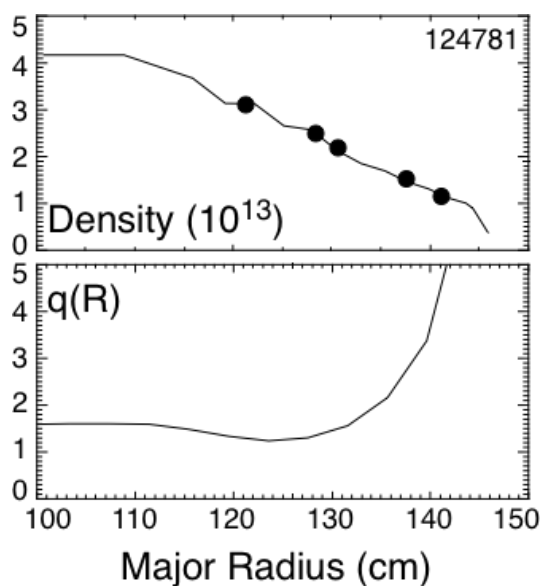


Fig. 2 Density and q profile at time of avalanche. Black dots indicate cut-off densities for reflectometer channels.

30 kHz to 200 kHz is shown in Fig. 3b for the three deepest channels: red – 50 GHz, blue – 44.5 GHz and green – 42 GHz. In Fig. 3c is shown a similar figure comparing again the relative amplitude evolution of the 50 GHz channel, now to the magnetic fluctuation amplitude measured at the plasma edge with a Mirnov coil. In the final burst, the total amplitude of TAE activity increases roughly linearly by nearly an order of magnitude (Figs. 3b & 3c), the dominant modes show strong, roughly linear in time, downward frequency chirps and there is a drop in the volume neutron emission rate (Fig. 3e).

The structure of the modes does not change significantly, at least initially, as the modes grow. Just towards the end of the final burst (inset Fig. 3b) the mode amplitude deeper in the plasma (closer to the magnetic axis) grows relatively faster than towards the edge, suggesting that in the very non-linear state the mode structure becomes slightly more peaked. Again, in Fig. 3c, the relative magnetic and density fluctuation amplitudes track well, except at the very largest amplitudes where the (core) density fluctuation

amplitude increases faster than the (edge) magnetic fluctuation amplitude.

#### 4. Measurement of fast-ion redistribution and losses

Diagnostics for the study of fast-ion loss or redistribution on NSTX include the multi-channel neutral particle analyzer (NPA) diagnostics, fast neutron rate monitors and the scintillator-based fast lost ion probe (sFLIP). In Fig. 1b is shown the energy resolved, time-dependant NPA spectrum measured on a mid-plane chord with 60 cm tangency radius during the TAE avalanches. Bursts of signal, indicating redistribution of fast-ions, are seen at the time of each avalanche. Of particular interest is that the redistribution extends down to energies at least as low as 30 keV, less than half the full energy of injection. The sFLIP diagnostic does not detect fast-ion losses associated with the avalanche, but  $D_\alpha$  bursts are correlated with each avalanche and neutron drop, suggesting that lost fast ions are striking plasma-facing components, enhancing recycling.

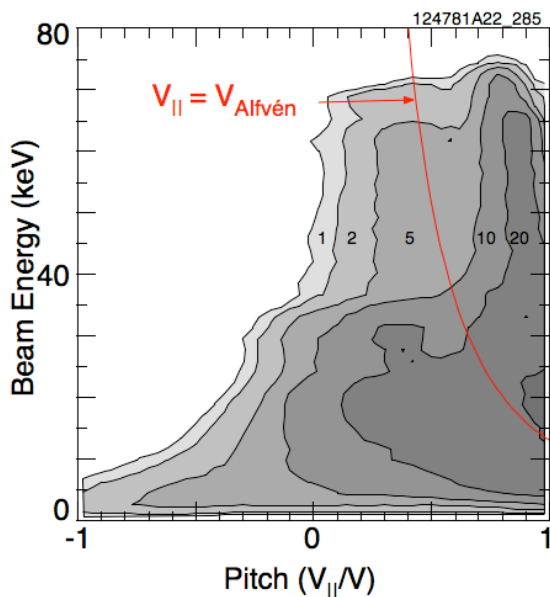


Fig.4. Fast ion distribution as calculated in TRANSP. Red line shows fast ion with parallel velocity equal to the Alfvén speed.

[6] (for stability) and ORBIT [7] codes (for fast ion transport). The fast-ion distribution vs. pitch-angle and energy as calculated in TRANSP, is shown in Fig. 4. This distribution is taken from the radius near the minimum in  $q$  and has a peak at full energy at a pitch,  $V_{||}/V \approx 0.75$ . The width (in pitch) of the peak broadens as the ions slow down due to pitch-angle scattering. Nearer the magnetic axis the peak at full energy in pitch is  $\approx 0.5$  and is closer to 0.9 at the plasma edge. The red line in the figure shows where  $V_{||} \approx V_{\text{Alfvén}}$ ; beam ions with energies above the line can still meet the parallel resonance condition. These fast-ion distributions do not incorporate the effect the TAE or TAE avalanches have had on fast-ion transport.

The mode structure and fast ion transport are modeled with the NOVA and ORBIT codes. The NOVA and ORBIT calculations use the reconstructed plasma equilibrium, the fast ion distribution and the kinetic pressure profile, now including thermal ion and electron, as well as the fast-ion pressure profiles, from TRANSP. NOVA is used to calculate the linear eigenmodes. The mode amplitude evolution must be scaled with experimental measurements and the mode frequency evolution for chirping modes must also be taken from experimental measurements. The eigenmodes, properly scaled, and

#### 5. Simulation of mode structures (NOVA) and fast ion transport (ORBIT)

The plasma equilibrium is reconstructed, constrained by MSE measurements of the magnetic field pitch-angle profile, and forms the basis for analysis using the TRANSP code. The beam deposition model in TRANSP is used to predict the distribution of fast-ions, to be used as input to the NOVA-k

the experimentally measured frequency evolutions are used in ORBIT which models the affect of the modes on fast ion transport.

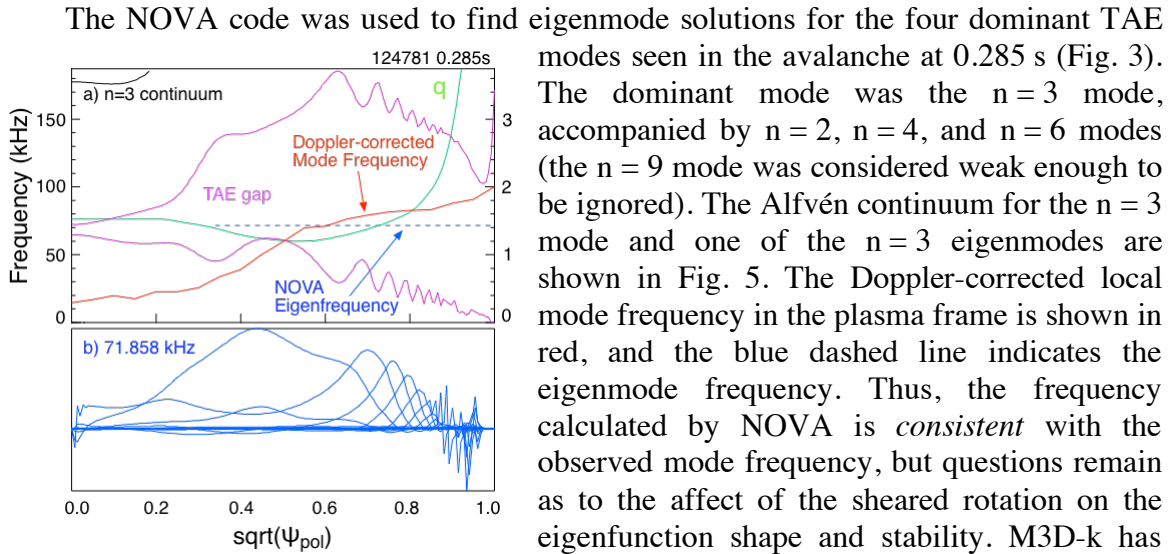


Fig 5. NOVA simulations for the  $n = 3$  mode at 0.285s. a) Magenta curves show TAE gap, green curve shows the  $q$ -profile (axis on right), red curve shows the local, Doppler-corrected mode frequency (plasma frame), dashed blue line shows NOVA eigenfrequency, b) poloidal harmonics of the  $n = 3$  mode at 71.9 kHz.

were chosen based on comparison of the radial mode structure of the NOVA eigenmodes with the multi-channel reflectometer measurements. For example, the simulated reflectometer responses for the five  $n = 3$  eigenmodes found by NOVA with frequencies between 67 kHz and 80 kHz are shown in Fig. 6. Three of the eigenfunctions were nearly degenerate, with frequencies between 79.4 kHz and 80.1 kHz (orange, purple and red curves), and very similar radial eigenfunction shape. the best match to the measured radial eigenfunction shape (blue squares) is the NOVA eigenmode with frequency of 71.9 kHz (blue dashed line). The solid blue line is the actual plasma displacement summed over the poloidal harmonics on the outboard midplane. The eigenmode with frequency of 69.7 kHz (green curve) is clearly a poor match. A similar analysis was done for each of the observed modes to select the eigenfunctions for use in ORBIT. The reflectometer response was simulated with the O-mode 1-d wave equation.

The ORBIT code is used to calculate the guiding-center orbits of fast ions in the experimental equilibrium using the linear eigenmode structure for the  $n = 2$ ,  $n = 3$ ,  $n = 4$  and  $n = 6$  modes as simulated with NOVA. The measured TAE mode amplitude and

NOVA found multiple solutions for each of the observed toroidal mode numbers. The eigenfunctions used in the ORBIT calculations

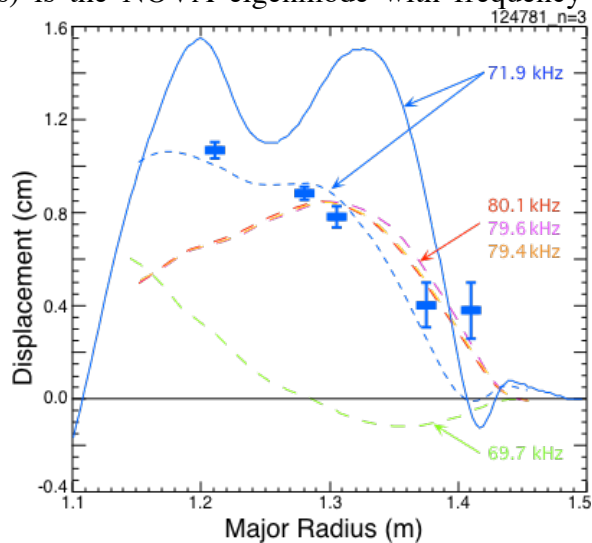


Fig. 6. a) NOVA displacement on outboard midplane (solid blue), synthetic reflectometer response (dashed curves) found by solving the 1-D O-mode equation on the midplane. experimental data (blue squares).

### EX/6-3

frequency evolutions for each of the modes over the 1 ms of the final, large avalanche burst were used in the simulation. The amplitude evolutions of the  $n = 3$  and the  $n = 6$  modes were approximated with a linear ramp in time (cf. Fig. 3b or 3c), and the frequency evolution was modelled with a linear downward frequency chirp (Fig. 3a or 3d). The  $n = 2$  and  $n = 4$  mode evolutions were approximated with constant amplitude and frequency.

The ORBIT simulation found that roughly 12 % of the fast ions were lost during a simulated 1 ms burst, in good agreement with the observed drop in the neutron rate of 12% to 15%. The losses are distributed over a broad range of energies and pitch angles, qualitatively consistent with the NPA data which indicated redistribution of fast ions over a range of energies from  $\approx 30$  keV up to full energy of  $\approx 70$  keV. This redistribution was also seen on multiple NPA chords which are sensitive to a range of pitch angles.

The NSTX TAE avalanches exhibit at least two nonlinear features, the interactions of multiple modes, and the strong frequency chirps. The interactions of multiple modes can both result in an increase of mode amplitude as well as a nonlinear enhancement of fast ion transport due to island overlap in fast-ion phase space. The frequency chirps suggest the formation of phase space structures which drive the frequency of the modes away from their natural frequencies. ORBIT can investigate these non-linear features to a limited extent and most importantly, not self-consistently.

The sweeping of the mode frequency in time allows the mode to be resonant with, and cause transport of, a larger population of fast ions. ORBIT can model this effect, but the frequency sweep, driven in the non-linear physics through phase-space structures, must be included on an *ad hoc* basis by using the experimental data. An ORBIT simulation with no frequency chirping, that is with the frequencies of the  $n = 3$  and  $n = 6$  modes fixed at their initial values, found a loss of only  $\approx 8\%$  of the fast ion population, supporting the conjecture that frequency sweeping extends the resonant interaction of the mode to a larger fraction of the fast ion population. The ORBIT simulation is not, of course, self-consistent and the actual frequency chirp represents some natural feedback interaction between the fast ion population and the mode drive, which would tend to optimize the mode-fast ion interaction, absent in this simulation.

The interaction of multiple modes can also result in a non-linear enhancement of fast ion transport, and in an enhancement of the drive for each mode. The non-linear enhancement of the mode drive is again included in an *ad hoc* fashion by using the experimentally measured mode amplitudes. The island overlap can be modelled with ORBIT, but not in an entirely self-consistent manner. The dominant mode in the avalanche burst is the  $n = 3$  mode. An ORBIT simulation including only the  $n = 3$  mode results in a net fast ion loss of  $\approx 11.6\%$ . A simulation including only the  $n = 2$ ,  $n = 4$  and  $n = 6$  modes results in a negligible loss of  $\approx 0.2\%$  of the fast ions. The sum of the losses from these two simulations is 11.8%, only slightly less than the 12.2% loss in the simulation with all of the modes. Thus, phase-space island overlap does not appear to play a significant role in these avalanche events.

## 6. Non-linear interactions of TAE with other modes

The non-linear interaction of multiple modes and frequency chirping in the avalanche events is through the fast ion distribution. Non-linear behaviors can also manifest through higher order terms in the dispersion equations. In some shots on NSTX it is found that the TAE become deeply trapped in the wave-field of a lower frequency, kink-like mode. The TAE become a wave-packet toroidally localized and stationary in the frame of a more

slowly rotating  $n = 1$  energetic particle mode (EPM). Thus, the TAE wave-packet and the EPM propagate together.

The wave-packet interpretation of the mode amplitude modulation is confirmed with the toroidal array of Mirnov coils. In Fig. 7 are shown the data from three Mirnov coils, separated toroidally by  $120^\circ$ . The data is digitally band-pass filtered to enhance the EPM (blue) and overlaid with the same data, now filtered to enhance the TAE wave-packets (red). As the kink mode rotates toroidally, the TAE wave-packet remains trapped at a fixed phase of the EPM.

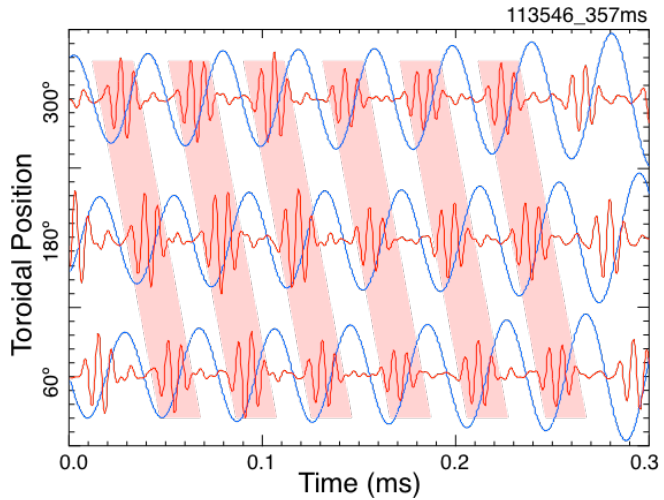


Fig. 7. Low pass (blue) and high pass (red) filtered Mirnov coil data showing TAE as wave packets trapped in EPM wave.

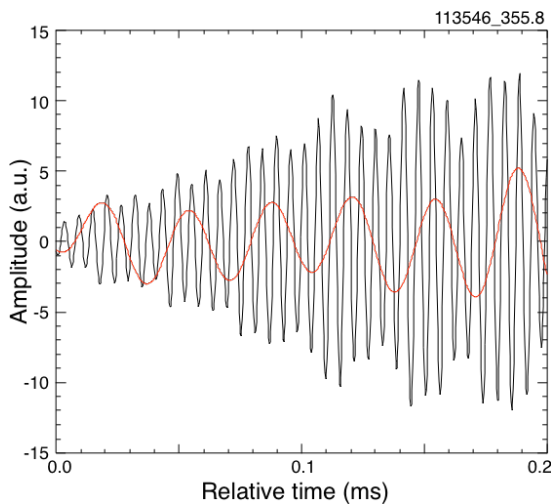


Fig. 8 Weak modulation of TAE at EPM onset.

roughly 50% of the peak amplitude, the modulation of the TAE amplitude approaches 100%, as seen in Fig. 7.

The observed wave-packet can be represented as the sum of many waves, with frequencies and mode numbers incremented by the frequency,  $\approx 20$  kHz, and the toroidal mode number,  $n = 1$ , of the EPM. Fourier analysis and mode identification of the Mirnov data, of course, finds multiple peaks in the spectrum with toroidal mode numbers from  $n = 3$  to  $n = 7$ . The interpretation that these observations are indicative of strong non-linear wave-wave coupling

In this example, both the EPM and the TAE are bursting. The neutron rate drops at each burst, suggesting that fast ions are lost, temporarily reducing the drive until the fast ion population can be replenished. The non-linearity of the interaction of the waves can be studied, then, as the EPM amplitude increases. Very early in the burst when the EPM amplitude is  $\approx 2\%$  of the peak amplitude (and the TAE amplitude is  $\approx 10\%$  of its peak amplitude), the EPM results in  $< 20\%$  modulation of the TAE amplitude (Fig. 8). When the amplitude of the EPM is

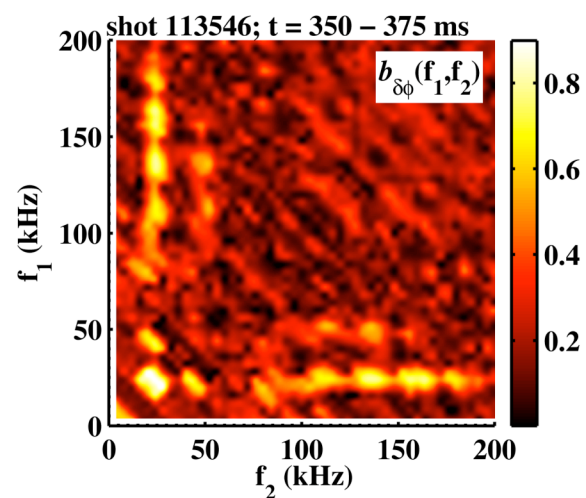


Fig. 9 Bicoherence of 50GHz reflectometer for  $t = 350$  to  $375$  ms. Max. uncertainty  $\approx 0.1$ .

may be tested with bi-coherence analysis (Fig. 9). The strong bi-coherence between the  $n = 1$  EPM and the multiple modes (wave-packet) in the TAE frequency band are proof of three-wave coupling. Future work will try to identify the nature of the non-linearity, perhaps explaining why it is not always present and whether the bunching of the TAE into wave-packets affects the induced fast-ion transport in some significant way.

The slowly-growing EPM, on the time scale of the TAE wave, can be viewed as a helical equilibrium, such as in a stellarator. However, even at full amplitude the equilibrium is nearly axi-symmetric. Thus the origin of the strong interaction between the TAE and EPM shown here is somewhat mysterious. In future work we hope to use codes developed to study fast ion instabilities in stellarator geometry to model these plasmas.

## 7. Summary

In this work we have demonstrated that the NOVA and ORBIT codes can provide reasonable, qualitative models of the TAE structure and fast-ion losses. The NOVA code found eigenmodes with frequencies and radial structure matching the experimental measurements. The linear eigenmode amplitudes were scaled to match the experimental measurements and the mode frequencies are matched to the experimental spectra. With these modes, the ORBIT code predicts a loss of  $\approx 12\%$  of the fast ion population through the final avalanche burst, in agreement with the 10% to 15% drop in neutron rate. The agreement between NOVA/ORBIT modelling here and experimental measurements of losses is surprisingly good in light of previous attempts [cf. Ref. 8]. The avalanche on NSTX resulted in quite large modes with  $dn/n \approx 5\%$  with strong frequency chirping. The eigenfunctions on NSTX are also quite broad which enhances fast ion transport.

These simulations are not self-consistent. They demonstrate that the linear modelling of the Toroidal Alfvén eigenmode reasonably models even the non-linear mode. The simulations also suggest that much of the physics of the strongly non-linear multi-mode interaction incorporated in the avalanche model can be captured with the ORBIT code – as long as the experimental data is there to guide the non-linear mode behaviours (growth rates, unstable modes, frequency chirping). However, this knowledge is of limited value for predicting whether avalanches will be present under different, *e.g.*, ITER, conditions. This will require the development and benchmarking of fully non-linear codes such as M3D-k which can predict saturation amplitudes and frequency evolution.

Work supported by U.S. DOE Contracts DE-AC02-76CH03073, DE-FG03-99ER54527, DE-FG02-06ER54867, and DE-FG02-99ER54527.

## References

- [1] M. Ono, S M Kaye, Y-K M Peng, *et al.*, Nucl. Fusion **40** (2000) 557.
- [2] K L Wong, Plasma Phys. and Control. Fusion **41** PR1 (1999).
- [3] H. L. Berk, B. N. Breizman, M. Pekker, Phys. Plasmas **2**, 3007 (1995).
- [4] E.D. Fredrickson, N N Gorelenkov, R E Bell, *et al.*, Nucl. Fusion **46**, s926 (2006).
- [5] N. A. Crocker, *et al.*, Phys. Rev. Lett. **97** (2006) 045002.
- [6] N. N Gorelenkov, C. Z. Cheng, and G. Y. Fu, Phys. Plasmas **6** (1999) 2802.
- [7] R. B. White and M. S. Chance, Phys. Fluids **27**, 2455 (1984).
- [8] W. W. Heidbrink, M. A. Van Zeeland, *et al.*, Nucl. Fusion **48** (2008) 84001.